Radar Sensors in Collaborative Robotics: Fast Simulation and Experimental Validation

Christian Stetco[1], Barnaba Ubezio[2], Stephan Mühlbacher-Karrer[2], Hubert Zangl[1]

***Abstract*— With the availability of small system in package realizations, radar systems become more and more attractive for a variety of applications in robotics, in particular also for collaborative robotics. As the simulation of robot systems in realistic scenarios has become an important tool, not only for design and optimization, but also e.g. for machine learning approaches, realistic simulation models are needed. In the case of radar sensor simulations, this means providing more realistic results than simple proximity sensors, e.g. in the presence of multiple objects and/or humans, objects with different relative velocities and differentiation between background and foreground movement. Due to the short wavelength in the millimeter range, we propose to utilize methods known from computer graphics (e.g. z-buffer, Lambertian reflectance model) to quickly acquire depth images and reflection estimates. This information is used to calculate an estimate of the received signal for a Frequency Modulated Continuous Wave (FMCW) radar by superposition of the corresponding signal contributions. Due to the moderate computational complexity, the approach can be used with various simulation environments such as V-Rep or Gazebo. Validity and benefits of the approach are demonstrated by means of a comparison with experimental data obtained with a radar sensor on a UR10 arm in different scenarios.**

I. INTRODUCTION

The detection of objects in the vicinity of both mobile and stationary robots becomes ever more important, in particular when robots share the space in which they operate with humans (see Fig. 1). Actually, it is not just about detection - knowledge of the pose, shape and relative velocity of the objects in the near surrounding of robots plays a major role for safe and efficient motion planning. Proximity perception addresses the acquisition and representation of the related information. Humans use a sensor fusion approach with a strong emphasize on vision for proximity perception. Nevertheless, other information obtained form sources such as sound, thermal radiation, movement of air etc. is also used. Technical systems can augment the perception with additional non-contact sensing principles that go beyond the sensing capabilities of humans. Such principles include, e.g. optical, vision, capacitive, ultrasound and radar systems.

In order to have wide applicability, the size and weight of such sensors is crucial and a variety of principles can be considered for proximity perception, e.g. solid state optical phased array Light Detection And Ranging (LIDAR) [1], miniaturized 3D ultrasound sensors [2], miniaturized Time of Flight (ToF) cameras (e.g. [3]). Printed thermal radiation sensors [4] and capacitive sensors [5]–[7] offer the advantage of very low thickness of the sensor elements, but have limited spatial resolution and range.

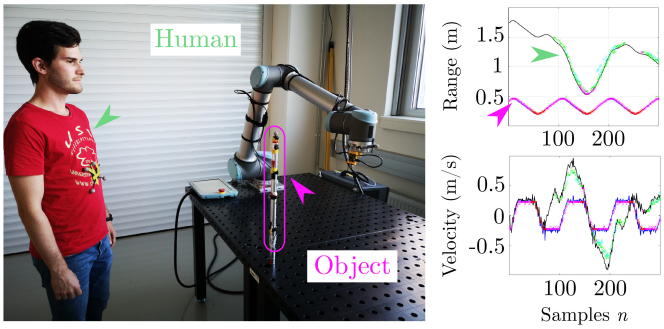

Fig. 1: Radar system towards collaborative robotics: With the radar sensor mount on the robot, the relative distance and relative velocity of objects can be determined. The setup shows a moving human and a stationary cylinder, the robot arm itself is also moving. The plots show the determined relative distances (top right) and relative velocities (bottom right) for both with respect to the robot arm as obtained from the radar sensor and as obtained from a optical reference system. The small differences demonstrate the accuracy of the radar system.

Radar systems offer many advantages compared to other sensor principles. They allow to directly determine distance and velocity of objects in their field of view. In comparison to optical and vision based systems, they are rather insensitive towards staining and surface scratches. Radar sensors can be covered by a protective layer, which also allows invisible installation of the systems, as the radar signals can pass through non-conductive materials.

FMCW radars offer several advantages that make them in particular useful for collaborative robotics. They are well suited for solid state integration and thus of miniaturized realization. Several radar sensors can be used in the same space with minimal interference due to a comparatively easy separation in frequency and time domain. They provide high resolution and simultaneous measurement of distance and velocity also for short ranges. Consequently, they can be utilized in proximity perception, collision avoidance and

[1] The authors are with the Institute of Smart System Technologies, Sensors and Actuators Department, Alpen-Adria-Universität, Klagenfurt am Wörthersee 9020, Austria, E-Mail: {christian.stetco,hubert.zangl}@aau.at

[2] The authors are with the Institute of Robotics and Mechatronics, JOANNEUM RESEARCH ROBOTICS, Klagenfurt am Wörthersee 9020, Austria, E-Mail: {Barnaba.Ubezio, Stephan.Muehlbacher-Karrer}@joanneum.at

human robot interaction like in gesture recognition.

With the availability of small radar systems that can even include antenna arrays within the chip package, radars have become attractive for many applications in proximity perception. Sensor chips no larger than a finger tip have successfully been used in gesture based human machine interaction e.g. with wrist watches or mobile phones [8], [9].

A. Related Work

In the field of autonomous and mobile robotics, radar sensors are commonly used for navigation and mapping [10]. Millimeter-Wave (mmW) radars have been successfully exploited by several research teams, for applications such as Simultaneous Localization and Mapping (SLAM) [11], [12], because of their advantageous operation capabilities in the long sensing range, as well as in harsh outdoor environments, e.g., night, fog and similar. Radar sensors are state of the art in Advanced Driver Assistance Systems (ADAS) [13], such as automotive Adaptive Cruise Control (ACC) systems, and in research for autonomous driving, e.g., [14], [15].
Recently, in [16] the radar sensor technology was also transferred to indoor mobile robot platforms: a PR2 Robot operates a mmW radar sensor with external antennas in the k-band (15-26.5 GHz) for 2D and 3D imaging, as a complement to optical sensors such as depth cameras.
Investigations towards safety aspects, in order to monitor the operation range of a robot based on an FMCW radar have been done in [17].

Thanks to further improvements, obtained by shrinking the size and integrating the antenna array on the sensor chip, mmW radar technology has become very attractive also for proximity perception [9], [18], [19]. 160 GHz radar with flexible waveguides and multiple antennas have been analyzed for proximity perception for collaborative robots [20], with corner reflectors utilized as targets. However, this configuration is in practice not suitable in a shared human robot environment.

As simulations have become very important for research in robotics, e.g. with respect to generate synthetic yet realistic training data for machine learning, also accurate simulation models of mmW radar systems that are suitable for the integration in robot simulation environments are of major interest. Due to complexity of geometries, analytic solution of the well-known Maxwell equations is usually not possible and numerical approaches such as Finite Element Time Domain or (FETD) [21] or Finite Differences Time Domain (FDTD) [22] have to be used. However, while providing rather accurate results, these approaches require high computational effort and are thus time consuming (e.g. [23]), as the short wave length of mmW radar requires fine discretization of the geometry.

Research towards real time simulation models for radars actually has a long history (e.g. [24]) and radar simulations have been developed for various domains, e.g. meteorology (e.g. [25]), geoscience (e.g. [26]) and the automotive domain (e.g. [27])). Instead of solving the full Maxwell equations, approximations are used, including approaches based on geometrical optics [28] and in particular ray tracing, e.g. for the computation of the so-called radar cross section of an object [29].

B. Contribution

We present a simulation approach for FMCW radar systems that is capable of providing realistic raw data for FMCW radars in various scenarios. The validity of the approach is demonstrated by comparison of simulation and experimental results using an optical marker based system for reference measurements ("ground truth"), with a radar system integrated on the flange of a UR10 robot arm, as shown in Fig. 1.

Advantages of the suggested approach are:

- Easy integration into existing simulation frameworks.
- As the approach uses standard methods from computer graphics to determine depth maps and shading, fast algorithms and hardware acceleration can be utilized.
- As the approach generates raw data similar to actual radar sensors, it can be used to develop and study signal processing algorithms including machine learning approaches.
- Radar parameters such as chirp rate, number of chirps, field of view, beam forming, etc. can easily be adjusted. It is also suitable to study benefits and drawbacks of certain configuration even before actual hardware becomes available. Therefore, it can also support the development of integrated circuit design, as requirements can be derived from the simulations.

The remainder of this paper is structured as follows: In Section II the concepts of FMCW radar systems is revised with the corresponding signal processing. The proposed simulation approach is described in Section III. Section IV describes the used experimental setup and compares the experimental result with the simulation results. Finally, in Section V a conclusion is given.

II. FMCW RADAR

A. Sensing Principle

FMCW radars are based on electromagnetic wave propagation and can be fully described by Maxwell's equations. FMCW methods typically use linear chirp signals at the transmitter side. The propagated wave will be reflected by obstacles and the reflected waves are captured by receiver antennas. Antenna arrays can be used for electronic beam steering. Fig. 2 shows the typical system block diagram of a FMCW radar.

The transmitted signal can be mathematically modeled as a linear chirp

$$s(t) = Ae^{j\left(\omega t + \frac{2\pi}{2} K t^2\right)} + A^* e^{-j\left(\omega t + \frac{2\pi}{2} K t^2\right)} \qquad (1)$$

where $K = \frac{B}{T_s}$ is the chirp rate and $\omega = 2\pi f_T$ is the lower chirp frequency. B is the bandwidth of the chirp signal and defined as $B = f_u - f_d$; T_s is the chirp duration and A the signal amplitude.

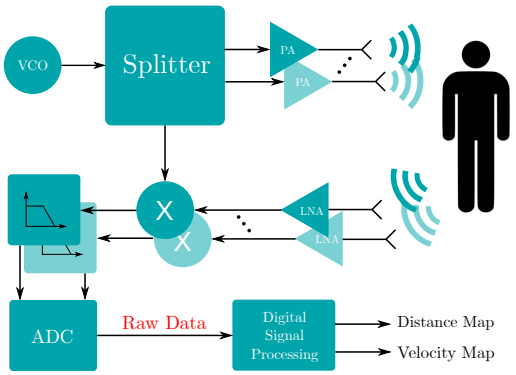

Fig. 2: Typical system block diagram of an FMCW radar module with multiple antennas. The transmitted radar signal gets reflected by objects. In the receiver, the received signal is mixed with the transmitter signal and low pass filtered. After Analog-to-Digital Conversion (ADC), raw data is provided in digital form. With signal processing, the distance and velocity are determined. The radar beam can be steered mechanically, or electronically by the used of several antennas as illustrated.

In the simplest case with only one reflection on one surface with uniform distance $d(t)$, the received signal is a time delayed and scaled copy:

$$\begin{aligned} s_R(t) = Be^{j\left(\omega(t-\tau)+\frac{2\pi}{2}K(t-\tau)^2\right)} \\ + B^* e^{-j\left(\omega(t-\tau)+\frac{2\pi}{2}K(t-\tau)^2\right)} \end{aligned} \tag{2}$$

where τ (or actually $\tau(t)$) is the time delay given by the ratio between distance $d(t)$ at time t and the speed of light c_0, such that τ is given by

$$\tau(t) = 2\frac{d_0 + vt}{c_0} \tag{3}$$

for an initial distance d_0 and a constant relative velocity v.

After mixing with the transmitter signal and low-pass filtering of the received signal to remove high frequency mixing products, one obtains the signal

$$\begin{aligned} s_M(t) =& AB^* e^{j\left(2\tau(\omega+2\pi Kt-\frac{2\pi}{2}K\tau)\right)} \\ &+ A^* B e^{-j\left(2\tau(\omega+2\pi Kt-\frac{2\pi}{2}K\tau)\right)} \end{aligned} \tag{4}$$

The instantaneous angular frequency is the time derivative of the exponent. Neglecting the small last term, one obtains

$$f_s(t) = \frac{1}{c_0}(2\frac{\omega}{2\pi}v + 2Kd_0 + 4Kvt) \tag{5}$$

The first term corresponds to the classical Doppler shift, the second depends on the distance, the third represents the change of the frequency due to movement, which is often neglected. In cases where the chirp rate K is fast enough, the Doppler shift might be negligible. However, when this is not the case, different approaches can be applied to separate velocity and distance dependent contributions. Using a positive and a negative chirp allows to separate both terms, as the sign of the distance dependent term is different for positive and negative chirp signals. Another approach is to utilize the third term, i.e. the time dependency of the frequency. While the first two terms are not time dependent, the change is due to the third term. Consequently, the velocity can be determined from the change of the frequency over time as described in Section II-B).

B. Distance and Velocity Estimation

To estimate the distance to a *single static* object, a single Fast Fourier Transform (FFT) operation can be used to determine the beat frequency of the demodulated signal $s_M(t)$. When several objects are within the range of the radar system at different distances, the FFT will show several peaks corresponding to the respective distances. Applying another FFT to the frequency components of a sequence of FFT results allows to determine the velocity of an moving object. Fig. 3 shows typical chirp signals obtained from a radar with corresponding frequency and range-velocity map.

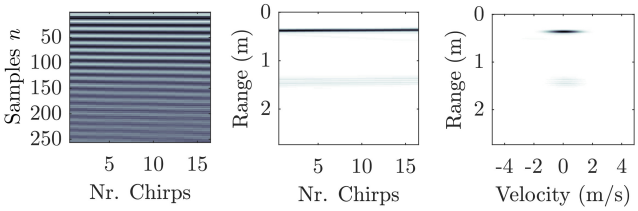

Fig. 3: Illustration of the signal processing to obtain distance and velocity. The sequence of raw signals (left, one column corresponds to the time signal for one chirp) an FFT applied to each column (middle). The peaks in this plot correspond to the distance of the objects. Applying an FFT over the sequence of the chirp FFTs allows to determine the velocity of each object. The corresponding plot (right) therefore shows distance and velocity of moving objects.

C. Radar Hardware Description

The sensor used for the experiments is the 60 GHz multi-channel radar transceiver Infineon BGT60, shown in Fig. 4, interfaced with the Infineon XMC4500 board to provide USB communication to the host PC. During measurements, the radar generates frequency chirps in a configurable bandwidth from 57 GHz to 64 GHz, suitable for short range computations [9]; moreover, the user can control via software the transmitter power, sampling frequency and number of samples and chirps.

III. SYNTHETIC DATA GENERATION FOR MULTIPLE OBJECTS

A. Determination of Signal Contributions

The proposed simulation model approximates the radar system using a depth image of a scene as illustrated in Fig. 5. Each pixel of the depth image covers a certain solid angle; consequently, the signal power per pixel is independent of the distance. For each pixel, the signal gets reflected at the given

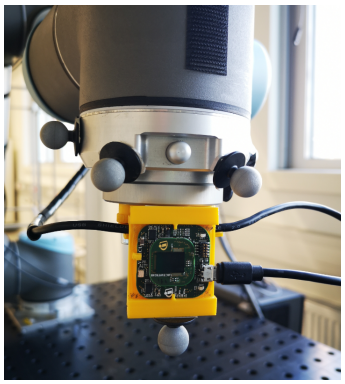

Fig. 4: Custom 3D-printed plastic support to hold the radar onto the robot flange. Optitrack markers are also mounted around the sensor to obtain reference measurements.

distance with a certain reflectance. The transmitted signal power, i.e. the radiant intensity P, is proportional to AA^* and is send out into space, such that

$$P = \oint U(\phi, \theta) d\phi d\theta \tag{6}$$

where $U(\phi, \theta)$ corresponds to the radiated power per solid angle, i.e. the radiance intensity, which can be expressed by the power and the directivity of the emitter

$$U(\phi, \theta) = \frac{D(\phi, \theta) P}{4\pi} \tag{7}$$

When the wave approaches a surface boundary A_i (i.e. a change of the wave impedance), the power P_{Ai} that reaches this boundary is given by the integral of the radiance intensity over the solid angle S_i corresponding to the surface area A_i,

$$P_{Si}(\phi, \theta) = \int_{S_i} U(\phi, \theta) dS_i \tag{8}$$

Further assuming that the area and thus the considered solid angle goes towards zero, the distance d_i and the reflectance R_i towards the receiver antenna can be assumed constant over this solid angle. Then, the power at the receiver obtained from this area is given by

$$P_{rSi} = \frac{A_r(\phi, \theta)}{d_i^2} R(\phi, \theta) P_{Si}(\phi, \theta) \tag{9}$$

Note that P_{Si} and the effective antenna aperture A_r are characteristics of the radar antennas and do not depend on the object, therefore these can be combined into $\hat{K}(\phi, \theta)$:

$$P_{rSi} = \hat{K}(\phi, \theta) \frac{1}{d_i^2} R(\phi, \theta) \tag{10}$$

Since the power is converted into an electrical voltage signal given by $U = \sqrt{P/R}$, the signal contribution arriving as a reflection from this area is given by

$$s_{rSi}(t) = K(\phi, \theta) \frac{1}{d_i} \sqrt{(R(\phi, \theta)} s(t - \tau) \tag{11}$$

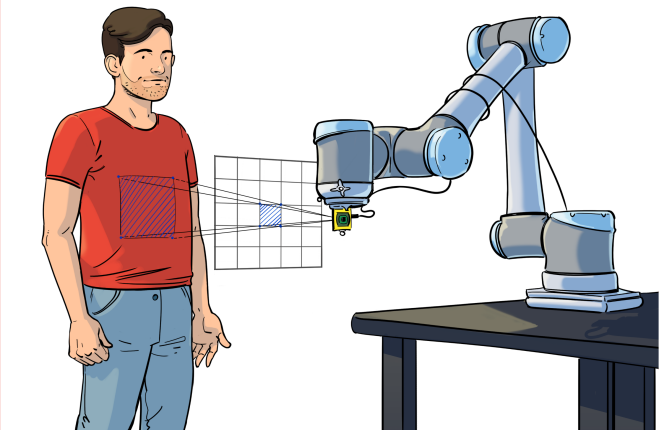

Fig. 5: Illustration of the proposed approach. A depth image is computed for the geometry. The signal power in each pixel does not depend on the distance of the object, as the corresponding area increases in the same way as the intensity decreases. However, the corresponding received reflected power by the area corresponding to one pixel scales with the square of the distance. The contributions from all pixels are weighted according to the directivity of receiver and transmitter antenna (array) and the reflection model, and then summarized to obtain the time signal corresponding to the raw data according to Fig. 3.

The integral to obtain the receiver signal is approximated using 2D discretization. Each pixel receives a certain power from the transmitter depending on the total power and the directivity in the direction of the pixel. As an approximation it is assumed that the distance over the pixel as well as the reflectance over the area corresponding to the pixel are constant. Consequently, the synthesized receiver signal s_M is obtained in analogy to the single object case from

$$\begin{aligned} s_M(t) = \sum_i \sum_j K_{ij} \frac{1}{d_{ij}} \sqrt{R_{ij}} \big(& e^{j\left(2\tau(\omega + 2\pi K t - \frac{2\pi}{2} K\tau)\right)} \\ & + A^* B e^{-j\left(2\tau(\omega + 2\pi K t - \frac{2\pi}{2} K\tau)\right)} \end{aligned} \tag{12}$$

where K_{ij} represents the transmitter and receiver characteristic with respect to the pixel, d_{ij} the distance for this pixel as obtained from a depth image with τ_{ij} as the corresponding time of flight (compare Eq. 3) and R_{ij} as the reflection coefficient for the surface covered by the pixel (compare Section III-B). The simulated ADC samples are obtained by evaluation $s_M(t)$ at the sampling times $s_M[n] = s_M(n\Delta T_S)$ with sampling interval T_S. The velocities are approximated by computing the depth map differences between two successive simulation steps

$$\vartheta_{\text{ij,k}} = \frac{(d_{ij,k} - d_{ij,k-1})}{\Delta t} \tag{13}$$

where Δt is the time difference between two simulation steps and $d_{ij,k}$ and $d_{ij,k-1}$ are the distances for the pixels

at simulation steps k and $k-1$. Hence, the chirp signals are generated by adjusting the distance values based on the introduced change in distance due to the velocity.

B. Reflection Model

Radar signals are partially reflected at boundaries between areas with different wave impedance and, depending on the material and boundary properties, both specular and diffuse reflection can occur. Modeling this behavior would require detailed knowledge of these parameters, which is often not available. However, as the main information on distance and velocity is represented in the frequency domain, the magnitudes are not that critical and it is therefore proposed to use approximate models and accepting issues such as limitation in the correct behaviour in situations with low signal to noise ratios. A common approach to model diffuse reflection as it occurs on rough surfaces is using Lambertian reflectance model [30]. In this model, the intensity in a certain direction is proportional to the scalar product of the face normal vector and the direction of the beam. Additionally, specular reflections may be added [31], i.e. an excessive reflection in a mirror like fashion, e.g. using Fresnel reflection coefficients. Both approaches are well established in computer graphics and standard rendering in a gray scale fashion can thus be used to obtain the relative reflectance with respect to the radar receiver. Consequently, both a grey scale image and a depth image are combined in the proposed approach for the radar simulation.

C. Simulation Setup

The environment including the UR10 robot, the human, the object as well as the radar sensor has been simulated using the robot simulation tool V-REP. It is worth noting that the proposed framework is not limited to V-REP but can be extended to other simulators, e.g. Gazebo. For the simulation of the radar sensor, one has to adjust the following parameters:

- Signal bandwidth
- Chirp rate
- Sample rate
- Number of chirps

Changing the values of these quantities allows to control detection range and accuracy of the radar, as well as the number of measurement data to process. Increasing the number of chirps increases the velocity resolution of the radar whereas adjusting the bandwidth allows to adapt the range resolution of the radar. In the simulation environment, a depth camera with an adjustable resolution of $N_p \times N_p$ pixels was used to acquire the raw depth information. Depending on the clipping of the depth camera, the raw camera data was scaled to distance values per pixel. Further signal generation and processing was done as described in Section II.

IV. EXPERIMENTAL SETUP AND RESULTS

For the experimental tests, we mounted the radar on the flange of a Universal Robot UR10 (see Fig. 4), a 6-Degree-of-Freedom (DoF) industrial robotic arm, suited for collaborative applications.

In order to have a versatile and reusable setup, we created a testbench where the robot is mounted on the edge of a table, onto which one or more targets can be positioned at known locations. The robot is then able to move freely in its environment, allowing the radar to adjust its field of view according to the targets' position.

For the ground truth we tracked both the radar sensor and the targets with special markers and a motion capture system from Optitrack [32]. A set of seven cameras, operating at a configurable working frequency, constantly measures the pose of each tracked object, with respect to a common reference frame, with sub-millimeter accuracy. It is then straightforward to compute the distance between radar and targets and, by operating on the working frequency, an estimation of the velocity of every object is also possible, gaining further data to use along the moving velocity imposed to the robot. From this, we designed a Robot Operating System (ROS) framework to perform several operations:

- Connect to the radar module and configure radar properties (transmitted signal power, chirp characteristics, number of samples, etc.).
- Connect to the Optitrack software to retrieve ground truth values.
- Start transmission and collect raw data, to be directly used in the simulation environment.
- Perform signal processing algorithms, such as FFT, in order to retrieve distance and velocity of the measured targets.
- Collect all data and compare with both the ground truth and the simulation results.

In our setup, the UR10 sends its joint configuration at a rate of 125 Hz, the radar provides distance and velocity estimates at a rate of 40 Hz, and the Optitrack provides every object's pose also at a rate of 40 Hz. While higher rates are possible for the cameras, the computation of the velocity in that case leads to false peaks and errors.

A. Human and Object movement test

A lot of applications involve robots interacting with objects in their workspace, e.g. for object manipulation. These kind of actions can proceed while a human operator collaborates with the robot in the scene; therefore, we created as a meaningful use-case scenario for both simulation and real measurement, a setup with a single static object on the table and a moving person approaching or moving away from the robot. This setup, shown already in Fig. 1 and in the video attachment, shows different advantages. For example, the human moves more randomly with respect to the robot, providing better coverage of different scenarios and sensor's measurement ranges. It also analyses a human-robot collaboration case, well suited for simulation environments as the one proposed in this paper. Human have more complex reflection properties than a standard-shaped object, giving more peaks with lower amplitude in the frequency spectrum; for example, the face and the chest will often result in two separate peaks, and the amplitude of each of these

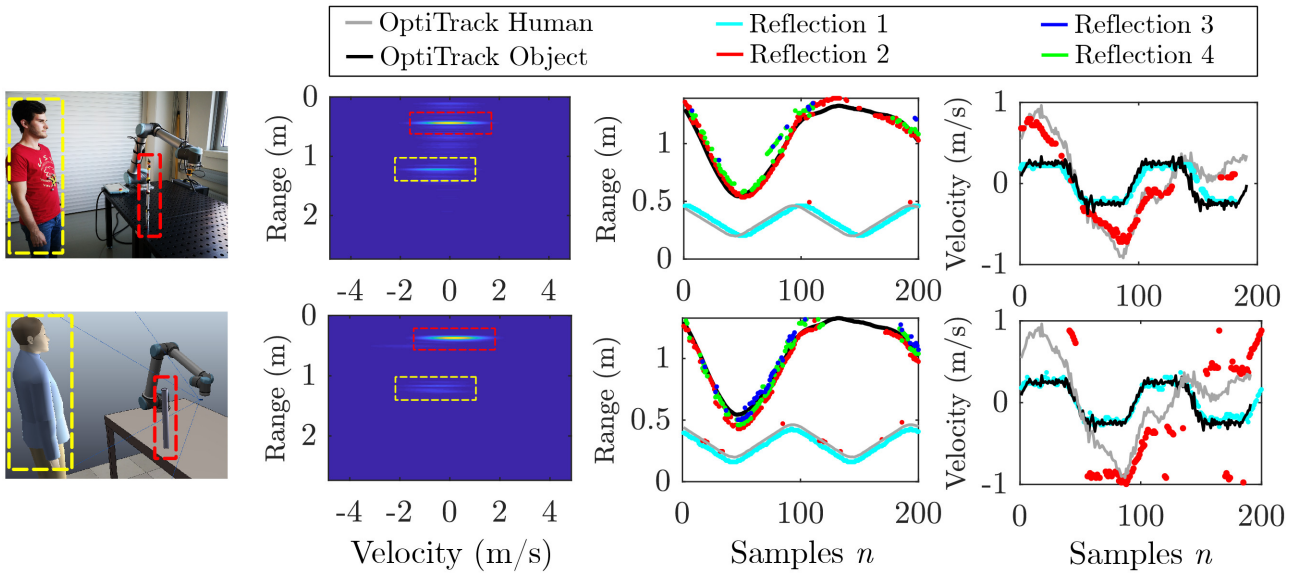

Fig. 6: Results of a human-object movement experiment. The top row shows the real data captured by the radar sensor for a scene as shown on the left. The bottom row shows the corresponding simulation data of the proposed framework. The red and yellow bounding boxes are the object and the human, respectively. Both velocity and range are captured from real measurements and simulation and a snapshot of the range-velocity map at sample $n = 200$ is shown in the left plot. The plot in the middle shows the obtain range estimates compared to the ground truth Optitrack values for a linear robot movement with speed $\vartheta_{UR} = 250mm/s$ and a human approaching and leaving the robot. The rightmost plot shows the estimated velocities, respectively.

peaks may vary with the specific movement. This results in more complex distance and velocity estimation than regular objects.

B. Results

Real measurement and simulated data are compared to check the validity of the simulation environment. Fig. 6 shows certain portions of the human-object movement. Since the object is static and the robot moves towards the object, the object reflects the strongest. Nevertheless, when the human approaches the robot, the radar captures multiple reflections, which are mapped to the human trajectory. This situation is also reproduced by the proposed simulation environment. Also, the velocity estimation of both the robot and the human can be reproduced by the simulation framework. The velocity estimation for the human is more challenging, for both measurement and simulation, due to the complex and strongly varying reflection pattern. The real and simulated estimates are in good accordance both with the ground truth and between each other.

V. CONCLUSION

In this paper we presented a simulation approach for FMCW radar sensors, in particular with respect to collaborative robotics and integration of short range radar systems on mobile and stationary robots into robot simulation environments such as V-rep or Gazebo. Based on methods from computer graphics, it can utilize fast algorithms and hardware acceleration and is thus capable to provide raw signals in real time. Current limitations of the proposed approach are ignorance of mirror-like reflections and multiple reflections along a beam path. Despite the fact that only a simple approximation of the refection properties is used, comparisons with experimental data show that the simulation results are in good accordance for both distance and velocity estimation for a wide range of scenarios. Therefore, the proposed approach provides much more realistic results for radar sensors than models that are typically available in robot simulation environments. As it can easily be integrated into such environments, it can be used to study, analyze and optimize radar systems on robots as well as to study, analyze and optimize the corresponding signal processing without the need to have a physical realization.

APPENDIX

The video attachment shows a variety of experiments conducted in the lab and the corresponding simulation results.

ACKNOWLEDGMENT

The research leading to this results has received funding from the ”Kärntner Wirtschaftsförderung Fonds” (KWF) and the ”European Regional Development Fund” (EFRE) within the CapSize project 26616/30969/44253. The authors would like to thank Matthias Brandl from Infineon Technologies AG for the support regarding the radar sensor and providing the BGT60 radar sensor. Finally, the authors would like to thank cartoonist Adriana Filippini for the picture shown in Fig. 5.

REFERENCES

[1] C. V. Poulton, A. Yaacobi, D. B. Cole, M. J. Byrd, M. Raval, D. Vermeulen, and M. R. Watts, "Coherent solid-state lidar with silicon photonic optical phased arrays," *Opt. Lett.*, vol. 42, no. 20, pp. 4091–4094, Oct 2017. [Online]. Available: http://ol.osa.org/abstract.cfm?URI=ol-42-20-4091

[2] N. Seckel and A. Singh, "Physics of 3d ultrasonic sensors," 07 2019.

[3] P. Fankhauser, M. Bloesch, D. Rodriguez, R. Kaestner, M. Hutter, and R. Siegwart, "Kinect v2 for mobile robot navigation: Evaluation and modeling," in *2015 International Conference on Advanced Robotics (ICAR)*, July 2015, pp. 388–394.

[4] C. Rendl, P. Greindl, M. Haller, M. Zirkl, B. Stadlober, and P. Hartmann, "Pyzoflex: printed piezoelectric pressure sensing foil," in *Proceedings of the 25th annual ACM symposium on User interface software and technology*. ACM, 2012, pp. 509–518.

[5] T. Schlegl, T. Kröger, A. Gaschler, O. Khatib, and H. Zangl, "Virtual whiskers — highly responsive robot collision avoidance," in *2013 IEEE/RSJ International Conference on Intelligent Robots and Systems*, Nov 2013, pp. 5373–5379.

[6] S. Mühlbacher-Karrer, M. Brandstötter, D. Schett, and H. Zangl, "Contactless control of a kinematically redundant serial manipulator using tomographic sensors," *IEEE Robotics and Automation Letters*, vol. 2, no. 2, pp. 562–569, April 2017.

[7] Fogale-Robotics, "Sensitive surfaces for human-robot interactions cooperation," http://www.fogale-robotics.com/, 2018.

[8] S. Wang, J. Song, J. Lien, I. Poupyrev, and O. Hilliges, "Interacting with soli: Exploring fine-grained dynamic gesture recognition in the radio-frequency spectrum," in *Proceedings of the 29th Annual Symposium on User Interface Software and Technology*. ACM, 2016, pp. 851–860.

[9] J. Lien, N. Gillian, M. E. Karagozler, P. Amihood, C. Schwesig, E. Olson, H. Raja, and I. Poupyrev, "Soli: Ubiquitous gesture sensing with millimeter wave radar," *ACM Trans. Graph.*, vol. 35, no. 4, pp. 142:1–142:19, Jul. 2016. [Online]. Available: http://doi.acm.org/10.1145/2897824.2925953

[10] M. Adams, M. D. Adams, and E. Jose, *Robotic navigation and mapping with radar*. Artech House, 2012.

[11] E. Jose and M. D. Adams, "Millimetre wave radar spectra simulation and interpretation for outdoor slam," in *IEEE International Conference on Robotics and Automation, 2004. Proceedings. ICRA '04. 2004*, vol. 2, April 2004, pp. 1321–1326 Vol.2.

[12] M. Chandran and P. Newman, "Motion estimation from map quality with millimeter wave radar," in *2006 IEEE/RSJ International Conference on Intelligent Robots and Systems*, Oct 2006, pp. 808–813.

[13] J. Ćesić, I. Marković, I. Cvišić, and I. Petrović, "Radar and stereo vision fusion for multitarget tracking on the special euclidean group," *Robotics and Autonomous Systems*, vol. 83, pp. 338–348, 2016.

[14] S. Clark and H. Durrant-Whyte, "Autonomous land vehicle navigation using millimeter wave radar," in *Proceedings. 1998 IEEE International Conference on Robotics and Automation (Cat. No.98CH36146)*, vol. 4, May 1998, pp. 3697–3702 vol.4.

[15] S. Chadwick, W. Maddern, and P. Newman, "Distant vehicle detection using radar and vision," in *2019 International Conference on Robotics and Automation (ICRA)*, May 2019, pp. 8311–8317.

[16] C. M. Watts, P. Lancaster, A. Pedross-Engel, J. R. Smith, and M. S. Reynolds, "2d and 3d millimeter-wave synthetic aperture radar imaging on a pr2 platform," in *2016 IEEE/RSJ International Conference on Intelligent Robots and Systems (IROS)*. IEEE, 2016, pp. 4304–4310.

[17] M. Zlatanski, P. Sommer, F. Zurfluh, and G. L. Madonna, "Radar sensor for fenceless machine guarding and collaborative robotics," in *2018 IEEE International Conference on Intelligence and Safety for Robotics (ISR)*, Aug 2018, pp. 19–25.

[18] S. Hazra and A. Santra, "Robust gesture recognition using millimetric-wave radar system," *IEEE sensors letters*, vol. 2, no. 4, pp. 1–4, 2018.

[19] Z. Flintoff, B. Johnston, and M. Liarokapis, "Single-grasp, model-free object classification using a hyper-adaptive hand, google soli, and tactile sensors," in *2018 IEEE/RSJ International Conference on Intelligent Robots and Systems (IROS)*. IEEE, 2018, pp. 1943–1950.

[20] M. Geiger and C. Waldschmidt, "160-ghz radar proximity sensor with distributed and flexible antennas for collaborative robots," *IEEE Access*, vol. 7, pp. 14 977–14 984, 2019.

[21] H. Liu, B. Xing, H. Wang, J. Cui, and B. F. Spencer, "Simulation of ground penetrating radar on dispersive media by a finite element time domain algorithm," *Journal of Applied Geophysics*, vol. 170, p. 103821, 2019. [Online]. Available: http://www.sciencedirect.com/science/article/pii/S0926985116307157

[22] I. Giannakis, A. Giannopoulos, and C. Warren, "A realistic fdtd numerical modeling framework of ground penetrating radar for landmine detection," *IEEE Journal of Selected Topics in Applied Earth Observations and Remote Sensing*, vol. 9, no. 1, pp. 37–51, Jan 2016.

[23] M. L. Stowell, B. J. Fasenfest, and D. A. White, "Investigation of radar propagation in buildings: A 10 billion element cartesian-mesh fetd simulation," in *2008 IEEE Antennas and Propagation Society International Symposium*, July 2008, pp. 1–4.

[24] R. L. Boyell and H. Ruston, "Hybrid techniques for real-time radar simulation," in *Proceedings of the November 12-14, 1963, Fall Joint Computer Conference*, ser. AFIPS '63 (Fall). New York, NY, USA: ACM, 1963, pp. 445–458. [Online]. Available: http://doi.acm.org/10.1145/1463822.1463869

[25] J. M. Haynes, R. T. Marchand, Z. Luo, A. Bodas-Salcedo, and G. L. Stephens, "A multipurpose radar simulation package: Quickbeam," *Bulletin of the American Meteorological Society*, vol. 88, no. 11, pp. 1723–1728, 2007. [Online]. Available: https://doi.org/10.1175/BAMS-88-11-1723

[26] J. C. Holtzman, V. S. Frost, J. L. Abbott, and V. H. Kaupp, "Radar image simulation," *IEEE Transactions on Geoscience Electronics*, vol. 16, no. 4, pp. 296–303, Oct 1978.

[27] L. Reichardt, J. Maurer, T. Fugen, and T. Zwick, "Virtual drive: A complete v2x communication and radar system simulator for optimization of multiple antenna systems," *Proceedings of the IEEE*, vol. 99, no. 7, pp. 1295–1310, July 2011.

[28] T. Fugen, J. Maurer, T. Kayser, and W. Wiesbeck, "Capability of 3-d ray tracing for defining parameter sets for the specification of future mobile communications systems," *IEEE Transactions on Antennas and Propagation*, vol. 54, no. 11, pp. 3125–3137, Nov 2006.

[29] K. Schuler, D. Becker, and W. Wiesbeck, "Extraction of virtual scattering centers of vehicles by ray-tracing simulations," *IEEE Transactions on Antennas and Propagation*, vol. 56, no. 11, pp. 3543–3551, Nov 2008.

[30] T. Brook, P. F. Driessen, and R. L. Kirlin, "Propagation measurements using synthetic aperture radar techniques," in *Proceedings of Vehicular Technology Conference - VTC*, vol. 3, April 1996, pp. 1633–1637 vol.3.

[31] D. Brunner, G. Lemoine, H. Greidanus, and L. Bruzzone, "Radar imaging simulation for urban structures," *IEEE Geoscience and Remote Sensing Letters*, vol. 8, no. 1, pp. 68–72, Jan 2011.

[32] OptiTrack, "Technical data," *Natural Point Inc.*, 2013.